EXPERIMENTAL COMPARISION OF REINFORCED CONCRETE BEAMS STRENGTHENED AGAINST BENDING WITH DIFFERENT TYPES OF CEMENTITIOUS-MATRIX COMPOSITE MATERIALS

Christian Escrig[a*], Lluís Gil[a], Ernest Bernat-Maso[a]

[a] *Department of Strength of Materials and Structural Engineering. Universitat Politècnica de Catalunya. Colom 11, 08222 Terrassa, Spain*

Abstract

Using composite materials for retrofitting existing reinforced concrete (RC) structures is showed as a promising technique that offers outstanding performances due to their high strength-weight ratio and the ease of their application. However, the use of organic resins brings some drawbacks that fabric-reinforced cementitious matrix materials (FRCM) avoid. In this work, five types of FRCM applied as flexural reinforcement are comparative studied. Results show that most of the strengthened beams tested up to failure were able to increase their flexural capacity and flexural stiffness, but decreased their ductility. Finally, a new methodology to study the cracking process is presented.

Keywords: *Textile, bending, strengthening, experimental, ductility, stiffness, cracking.*

1. Introduction

Fabric-Reinforced Cementitious Matrix (FRCM) is a structural strengthening technique commonly applied on masonry ([1,2]) or reinforced concrete elements ([3,4]). It is a low-weight solution that consist in synthetic or natural fibres arranged in a mesh, which constitute a unidirectional or bidirectional textile, embedded in an inorganic matrix. In this sense, the fact of not using organic matrices supposes an evolution regarding the traditional composite strengthening system, Fibre-Reinforced Polymer (FRP), because of all the drawbacks related with resins that this material presents [5].

Unlike its organic-based counterpart, there are very little experimental studies about the mechanical behaviour of reinforced concrete (RC) beams flexural strengthened with FRCM. First investigations carried out compared the performance of both type of composite materials as a bending reinforcement: Kurtz and Balagaru [6] tested RC beams strengthened with one layer of carbon reinforcement and Toutanji y Deng [7] did the same with more layers of strengthening textile. Both studies showed that cement-based strengthened beams behave similarly than FRP ones in terms of increasing flexural capacity and post-cracked flexural stiffness. However, they were observed some differences regarding the developed failure modes because of mechanisms to transmit the stresses. Nevertheless, Si Larbi et al. [8] did a similar investigation where FRCM offered similar increasing of the flexural capacities than FRP in the case of the service state limit, but developing lower performances considering the ultimate state limit. Concurrently to these studies, Brückner et al. [9] focused their investigations on testing slabs flexural retrofitted with 4 and 8 plies of glass FRCM. They observed that cement-based strengthening were able to develop all their capacity and broke by tensile failure, even with short anchorage lengths. Furthermore, it was noticed that the obtained ductility levels were higher than the minimum prescribed by reinforced concrete standards.

Many of the studies carried out centred their work on study the behaviour of the polypara-phenylene benzobisoxazole (PBO) textile as a withstand material of FRCM flexural strengthening. These were the cases

* Corresponding author:

Tel.: +34 937398728; fax: +34 937398994

e-mail address: christian.escrig@upc.edu

of Ombres [10] and Babaeidarabad et al. [11]. Both investigations led to similar conclusions: PBO-FRCM used as flexural strengthening provides to RC beams an enhancement of their flexural capacities and a reduction of their ductility, which depends on the number of applied layers. Other authors [12,13] compared the performances of PBO-FRCM with non-organic composites casted with carbon textiles, observing that PBO composite materials showed more effective on improving the flexural capacity of the tested beams. On the other hand, some researchers focused their investigations on the influence of the matrix on the mechanical behaviour of FRCM. In this sense, D'Ambrasi y Focacci [12] pointed out that constitutive matrices should be designed depending on the type of fibre of the grid, and highlighted the unfeasibility of design proper mortars according to their classical mechanical properties, i.e., compressive strength, tensile strength or elastic modulus. Subsequently, Elsanadedy et al. [14] emphasised the suitability of using mortars modified with polymers in the case of strengthen RC structures with basalt meshes.

Very little number studies compared the mechanical behaviour of several types of FRCM acting as a flexural strengthening of RC beams. First of them was carried out by Larrinaga et al. [15]. In this research, carbon, basalt and steel FRCM were used to retrofit low-strength concrete beams. Therein, steel composite strengthening performed the best in terms of increasing the flexural capacity of the specimens. Moreover, it was noticed that different aspects, such as the size of the mesh, the number of applied plies and the covering of the tows, have high influence on the results. The second comparative study consisted on strengthening scaled precasted beams with five different types of FRCM [16]. This investigation highlighted the influence of the size of the mesh for a proper impregnation of the textile by the mortar in order to prevent debonding failures between them.

In spite of these researches, it has not been found any experimental study which compares the performance of different combinations of meshes and matrices applied as bending reinforcement on RC beams casted with high strength concrete. Therefore, this paper presents a comparative analysis carried out on high-strength concrete beams flexural strengthened with various types of FRCM. To fulfil this aim, 11 RC full-scale beams were tested using five different FRCM composite materials as flexural strengthening. Mechanical properties, such as flexural capacity, ductility and flexural stiffness, are analysed. Moreover, a new methodology to analyse the cracking process is also presented and discussed

2. Materials and specimen preparation

2.1 Reinforced concrete beams

To carry out the experimental works, 11 beams were built with a lack of longitudinal steel reinforcement (Figure 1). These specimens, designated as M-beams, had a length of 4.40 m and a cross-section of 500 mm x 200 mm. The longitudinal reinforcement consisted of two bars of Ø10 mm installed on the top and the bottom and another two bars of Ø8 mm installed in the middle of the cross-section as skin reinforcement. The transversal reinforcement were distributed to avoid shear failures. These stirrups were bars of Ø8 mm separated 300 mm along the central 1.4 m of the beams and bars of Ø8 mm separated 200 mm at the beginning and at the end of the beams. All reinforcement bars were B500SD. Three different batches of concrete were used. Table 1 summarises the mechanical properties of the concrete and steel. These data were obtained according to the specifications included in EN 12390-1 [17], EN 12390-3 [18] and EN ISO 15630-1 [19].

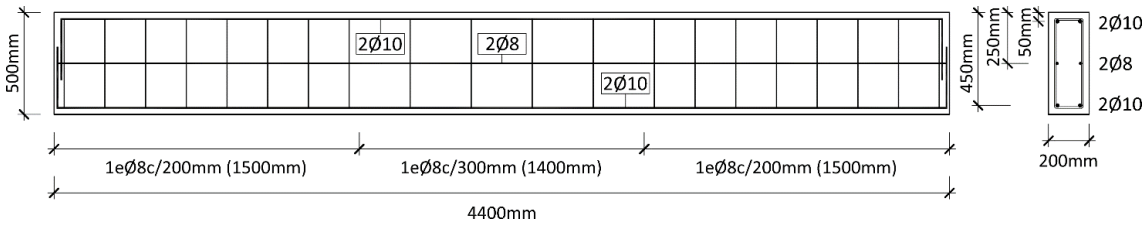

Figure 1. Geometry and steel reinforcement of the M-beams.

Table 1. Mechanical properties of the concrete and steel bars.

Concrete		***Steel***		
Cast batch	***$f_{cm,28}$ [MPa]***	***f_y [MPa]***	***f_u [MPa]***	***E_s [GPa]***
1	46.52			
2	42.35	517.20	633.63	198.48
3	55.42			

One of the M-beams was a control beam and the other 10 were strengthened with five different combinations of mortars and fabrics. Previously to be transported to the laboratory, all specimens were cured in ambient conditions for more than 30 days. It is important to highlight that four beams were flexural-cracked during the transport to the laboratory.

2.2 FRCM components

Mortars

Table 2 includes the mechanical properties of the FRCM mortar matrices used. Compressive and flexural strength were determined by standardized tests according to EN 1015-11 [20], tensile strength were calculated according to Bernat [21] and bonding strength values were obtained from the manufacturers, who used double-shear push tests to determine them. Four different mortars were used and described below:

- Mortar PHDM. Bicomponent mortar with high strength cement, glass fibres, selected aggregates and synthetic polymers in aqueous dispersion.
- Mortar R3. Hydraulic mortar modified with polymeric additions designed for structural repairing.
- Mortar XM25. Hydraulic puzzolanic mortar with additives compatible with masonry structures.
- Mortar XM750. Hydraulic mortar with fibres and special additives specifically designed to be applied on concrete.

Table 2. Mechanical properties of the mortars.

Mortar	***Compression strength (MPa)***	***Flexural strength (MPa)***	***Tensile strength (MPa)***	***Bonding strength*** (*) ***(MPa)***
PHDM	35.40 (2.53)	8.63 (0.57)	3.81 (0.57)	2.0
R3	24.65 (1.43)	8.13 (0.99)	3.59 (0.99)	-
XM25	24.95 (1.64)	7.87 (0.78)	3.47 (0.78)	0.8
XM750	30.02 (2.21)	10.65 (0.80)	4.70 (0.80)	-

Values in brackets indicate coefficient of variance.
(*) Values provided by manufacturer.

Fabrics

Five types of fabrics were used: basalt fibres (designated as B), carbon fibres (C), glass fibres (G), Poliparafenil-benzobisoxazole (PBO) fibres (P) and steel filaments (S) (Figure 2). Mechanical and

geometrical properties of fibres/filaments and fabrics are summarised in Table 3. Analysing these data, PBO and carbon fibres are those ones that present the highest ultimate tensile strength and Young's modulus, while basalt and glass are the fibres which have the highest ultimate strain. It is important to point out that PBO and steel fabrics work unidirectionally, while the others have the same properties in both principal orthogonal directions.

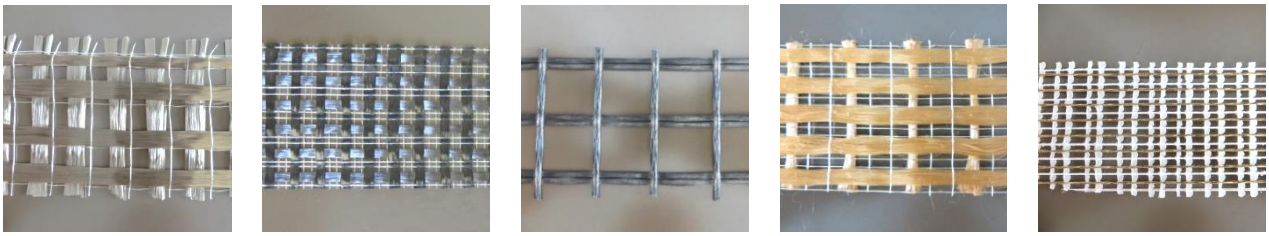

(a) (b) (c) (d) (e)

Figure 2. Strengthening fabrics: (a) basalt, (b) carbon, (c) glass, (d) PBO and (e) steel.

Table 3. Properties of the fibres and the fabrics.

Type of fibre			***Basalt***	***Carbon***	***Glass***	***PBO***	***Steel***
Designation			B	C	G	P	S
Fibres	*Fibre orientation* [a]		Bi	Bi	Bi	Uni	Uni
	Ultimate tensile strength	f_{fib} *[MPa]*	3080	4320	2610	5800	3200
	Young modulus	E_{fib} *[GPa]*	95	240	90	270	206
	Ultimate strain	ε_{fib} *[%]*	3.15	1.80	2.90	2.15	1.55
Fabrics [b]	*Weight*	w *(g/m²)*	200	168	225	88	600
	Wide of tow/cord	w_m *(mm)*	5.0	4.0	3.0	5.0	0.9
	Distance between tows/cords	s_m *(mm)*	15.0	10.0	25.0	10.0	5.5
	Equivalent thickness	t_{tex} *(mm)*	0.0530	0.0470	0.0420	0.0455	0.0750

[a] Bi=Bidirectional; Uni=Unidirectional.

[b] In the unidirectional case, the properties given are in the principal direction of the reinforcement.

FRCM

Five different combinations of fabrics and mortars were used to produce in situ FRCM flexural strengthening for the RC beams. All applied combinations followed the M-AB-C nomenclature, where A stands for the type of grid, B indicates the type of mortar, and C is the test repetition. In the case of the unstrengthened beam, the nomenclature was M-CONTROL. Table 4 summarizes the different specimens, FRCM combinations of the components and the batch of concrete.

Table 4. Tested specimens and FRCM combinations used as flexural strengthening of RC beams.

Specimen	***Textile***	***Matrix***	***Concrete batch***
M-CONTROL	-	-	2
M-BR3-01	Basalt	R3	3
M-BR3-02	Basalt	R3	3
M-CXM25-01	Carbon	XM25	2
M-CXM25-02	Carbon	XM25	2
M-GPHDM-01	Glass	PHDM	1
M-GPHDM-02	Glass	PHDM	1
M-PXM750-01	PBO	XM750	2
M-PXM750-02	PBO	XM750	2
M-SR3-01	Steel	R3	1
M-SR3-02	Steel	R3	1

2.3 Reinforcement application

One layer fabric of FRCM reinforcement system was applied as a flexural strengthening on the bottom face of the beams along 3.8 m length (Figure 3). With the aim of avoiding the debonding of the strengthening, two application methodologies were used. The first one consisted in increasing the adherence between the substrate and the FRCM mortar by removing the fine grain of the concrete surface using rough down techniques [22]. The second methodology was related with avoiding debonding failures at the end of the FRCM reinforcement. In this way, two U-jacket FRCM anchorages of the same material than the flexural strengthening (except in the case of steel fabrics where the anchorages were made of carbon grids) were applied (Figure 3) [15,12]. All strengthened beams were cured in laboratory conditions for at least 28 days prior to test.

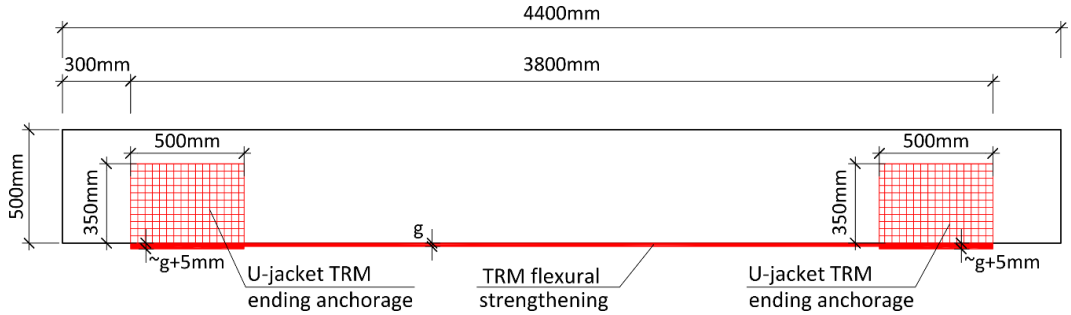

Figure 3. FRCM strengthening configuration on M-beams.

3 Methodology

3.1 Test set-up

All specimens were tested under a four-point flexural test with a free span between supports of 4.00 m, as it could be observed in Figure 4. The supports were metal cylinders that allowed free rotation in the plane of the beams. The load was applied using a hydraulic actuator and was transferred to the tested specimens through a steel distribution beam with two application points separated 1.40m between them. In all of the cases, this steel distribution beam was placed centred respect to the specimens and the supports. Tests were carried out under displacement control at 1mm/min until the displacement of the hydraulic actuator reached 20 mm. Since that, the test velocity was increased to 5 mm/min until the failure of the beams.

Vertical displacement was measured in five transversal sections. In three of them, corresponding to the centre of the beam and the mid-span between each load application point and their closest support, deflections were obtained using six potentiometers placed symmetrically by pairs on each side of the section. Deflections of the other two analysed sections, corresponding to the load application points, were controlled by laser position sensors (Figure 4a and Figure 4b).

Four strain gages were installed on the bottom side of the specimens oriented according the main direction of the tensile stresses (Figure 4a) to analyse the behaviour of the strengthened beams during the cracking process. These strain gages were 120 Ω resistance, 50 mm of measuring length and a gage factor of 2.08 ± 1.0%. Moreover, in order to identify different crack patterns accurately, grids of 125 mm x 125 mm were drawn on the surface of the specimens previous to test (Figure 4b). All data were continuously recorded at a frequency of 50 Hz using a data acquisition system.

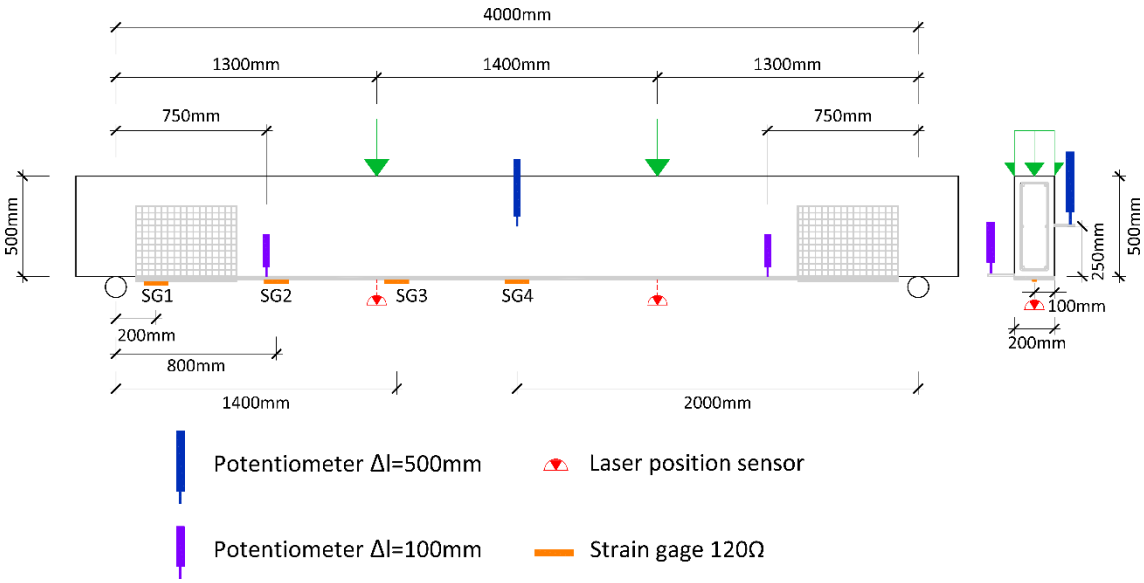

(a)

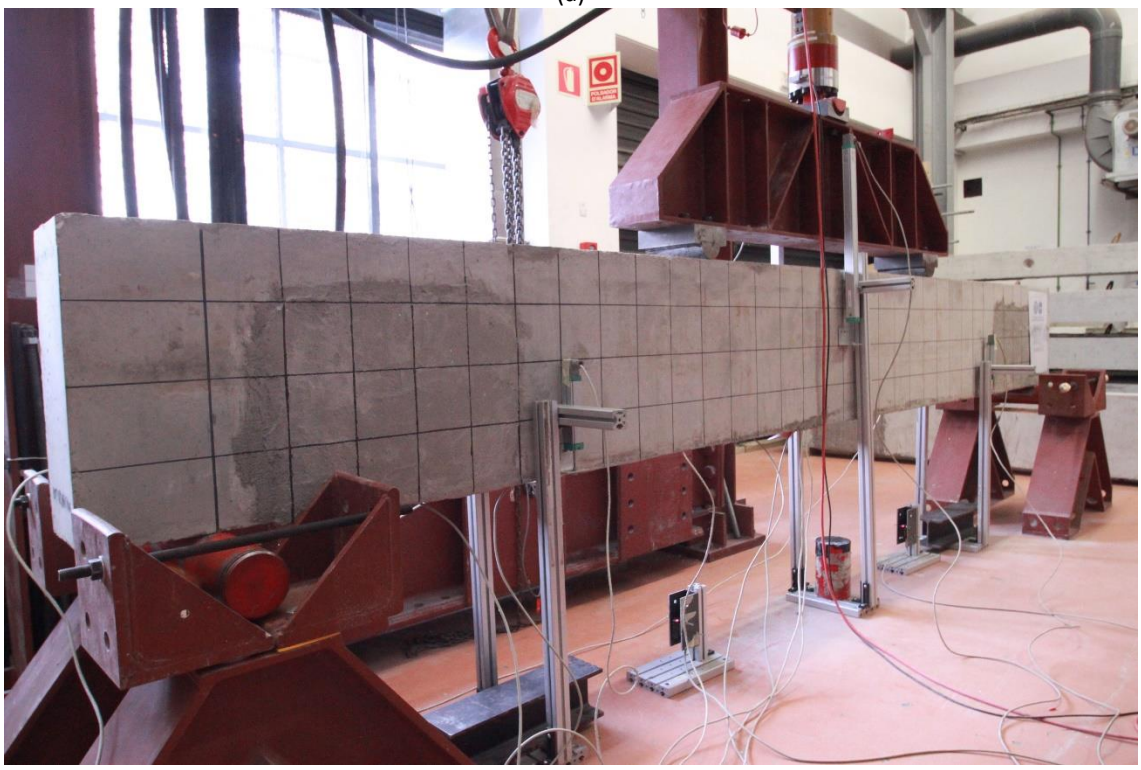

(b)

Figure 4. Test set-up: (a) sketch, (b) picture.

3.2 Analysed variables

According to the obtained data, four different aspects of the mechanical behaviour of the specimens were analysed: (1) flexural capacity provided by the FRCM strengthening, (2) ductility, (3) flexural stiffness and (4) cracking process of the tested beams.

Regarding the study of the flexural capacity of the FRCM strengthening, the bending moment versus mid-span deflection diagrams were acquired, obtaining from them the experimental values of the ultimate flexural moment ($M_{u,exp}$), the yielding flexural moment ($M_{y,exp}$) and the acting flexural moment at first-crack ($M_{cr,exp}$). Furthermore, with the aim of evaluating the effectiveness of the FRCM reinforcing systems, the normalized increment of ultimate flexural moment ($\Delta M_{tex,u}$) and the normalized increment of yielding flexural moment ($\Delta M_{tex,y}$) are defined according to Eq. 1 and Eq. 2, respectively. These parameters relate

the increment of the bending moment of the corresponding strengthened beams provided by FRCM reinforcement with the flexural capacity of each textile.

$$\Delta M_{tex,u} = \frac{M_{u,exp} - M_{u,exp}^{M-CONTROL}}{A_{tex} f_{fib} d_{tex}} \quad \text{Eq. 1}$$

$$\Delta M_{tex,y,j} = \frac{M_{y,exp} - M_{y,exp}^{M-CONTROL}}{A_{tex} f_{fib} d_{tex}} \quad \text{Eq. 2}$$

Where $M_{u,exp}^{M-CONTROL}$ and $M_{y,exp}^{M-CONTROL}$ are the experimental ultimate flexural moment and the experimental yielding flexural moment of the unstrengthened beam, respectively; A_{tex} is the area of the fibres included in the cross-section of each FRCM reinforcement according to Eq. 3; f_{fib} is the ultimate tensile strength of each type of fibre included in Table 3; and d_{tex} is the corresponding effective depth of the textiles according to Eq. 4.

$$A_{tex} = t_{tex} b \quad \text{Eq. 3}$$

$$d_{tex} = h + \frac{g}{2} \quad \text{Eq. 4}$$

Where b and h are the width and the high of the beams, respectively; t_{tex} is the equivalent thickness of the textiles (see Table 3); and g is the thickness of the FRCM for each case of study. It is important to note that, in equations Eq. 1 and Eq. 2, $M_{u,exp}$ and $M_{y,exp}$ are in kNm, A_{tex} is in mm^2, f_{fib} is in MPa and d_{tex} is in m.

On the other hand, in order to quantify the security of the different specimens during their failure process, ductility (χ) of the tested beams was evaluated according to Eq. 5.

$$\chi = \frac{\delta_{u,exp}}{\delta_{y,exp}} \quad \text{Eq. 5}$$

Where $\delta_{u,exp}$ and $\delta_{y,exp}$ are the deflections recorded at mid-span of the specimens when the ultimate flexural moment and the yielding flexural moment were reached during the tests, respectively.

Concerning the flexural stiffness (EI), this property was analysed in three stages of the loading process, that is to say, during the linear elastic stage, post-cracked stage and post-yield stage. The transition points between the different stages corresponded to the experimental values of the acting flexural moment at first-crack ($M_{cr,exp}$), the yielding flexural moment ($M_{y,exp}$) and the ultimate flexural moment ($M_{u,exp}$), as it could see in Figure 5.

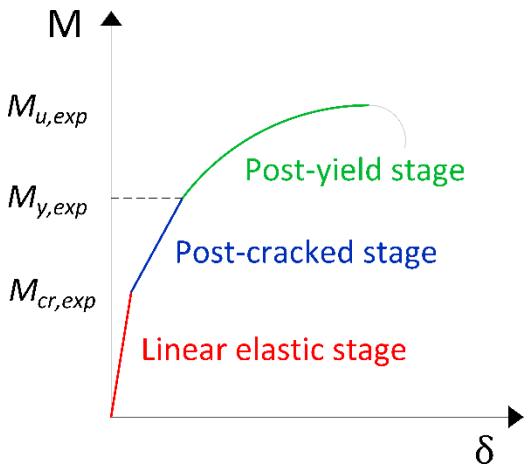

Figure 5. Stages where the flexural stiffness was analysed.

According to the test configuration (Figure 4), the flexural stiffness (*EI*) developed by the specimens can be expressed as following:

$$EI = \left(\frac{F}{\delta}\right)\left(\frac{a}{48}\right)(3L^2 - 4a^2) \qquad \text{Eq. 6}$$

Where *F* is the total applied load, which includes the load applied by the hydraulic actuator, the self-weight of the specimen and the weight of the steel distribution beam; δ is the vertical displacement at the mid-span section; *L* is the free span between supports (4000 mm); and *a* corresponds to the shear span (1300 mm) defined in the test set-up.

Despite the equation Eq. 6 was based on the principles that all constitutive materials of the specimens are lineal-elastic and the flexural stiffness remains invariable during the loading process, the flexural stiffness (*EI*) in the post-cracked and post-yield stages could be considered as an average effective flexural stiffness along the whole specimen [6,7]. In each stage, the term $\frac{F}{\delta}$ was obtained as the gradient of the idealized lines which best fitted the corresponding applied-force versus mid-span deflections diagrams. In the case of the present study, these lines are created joining the respective force frontier points ($F_{cr,exp}$, $F_{y,exp}$ and $F_{u,exp}$) calculated from their respective flexural moment values ($M_{cr,exp}$, $M_{y,exp}$ and $M_{u,exp}$).

Finally, the cracking development and the influence of the reinforcements on this process were studied thought a novel methodology by analysing the increasing of the acting flexural moment at first-crack because of FRCM ($\Delta M_{cr,FRCM}$) (Eq. 7). This is defined as the difference between the experimental value of the acting flexural moment at first-crack ($M_{cr,exp}$) and the theoretical value of the acting flexural moment at first-crack without taking into account the externally bonded reinforcement ($M_{cr,0}$) according to Spanish standard EHE-08 [23], as it could see in Eq. 8.

$$\Delta M_{cr,FCRM} = M_{cr,exp} - M_{cr,0} \qquad \text{Eq. 7}$$

$$M_{cr,0} = \frac{f_{ct,m}(t) I_{b,0}}{\frac{h}{2}} \qquad \text{Eq. 8}$$

Where $f_{ct,m}(t)$ is the average tensile strength of the concrete at the age of t days; $I_{b,0}$ is the total moment of inertia of the uncracked cross section of M-beams without considering the FRCM strengthening system, which can be calculated as a homogeneous rectangular section; and h is the height of the beam. According to the Spanish standard EHE-08 [23], the average tensile strength of the concrete at the age of t days ($f_{ct,m}(t)$) can be calculated from the average compressive strength of the concrete at 28 days ($f_{cm,28}$) as following (Eq. 9):

$$f_{ct,m}(t) = 0{,}3\sqrt[3]{(f_{cm,28}-8)^2}\, e^{\alpha s\left(1-\sqrt{\frac{28}{t}}\right)} \qquad \text{Eq. 9}$$

Where α is a coefficient which depends on the age of the concrete (for a concrete older than 28 days and characteristic compressive strength ($f_{ck,}$ see Eq. 10) lower than 50 MPa, this coefficient equals to 2/3); s is a coefficient which depends on the type of cement used to cast the concrete (in the case of this study, the used cement was CEM 42.5 and s takes the value 0.25); and t is the age of the concrete in days.

$$f_{ck}(t) = f_{cm,28} - 8 \qquad \text{Eq. 10}$$

4. Results

All beams were tested up to failure. In all the cases, the specimens developed the same flexural collapse where the main crack was occurred between the two load application points. The observed failure process consisted of (1) the appearance of flexural cracks and their propagation from the tensile side of the specimens until the neutral axis, (2) the yielding of the tensile steel and skin steel reinforcement, and the stretching of the FRCM grid, (3) the rupturing of the tensile steel and skin steel reinforcement and (4) the rupturing of the FRCM grid and the crushing of the concrete in compression. These phenomena were observed in the cross section failure where the main crack was developed. Despite the failure mode was equal for all the tested beams, it was observed three different cracking patterns described as follows:

A. Appearing and opening of numerous cracks approximately equidistant between them. Developing of the main crack at the end of the loading process.
B. Appearing of numerous cracks, but only two of them opened. One of the opened cracks became the main crack.
C. Appearing of numerous cracks, but only one of them opened. This crack became the main one.

Figure 6 shows the observed cracking pattern of all tested beams. For each beam, the main crack (in red), the opened cracks (in blue) and the appeared cracks (in green) are

highlighted.

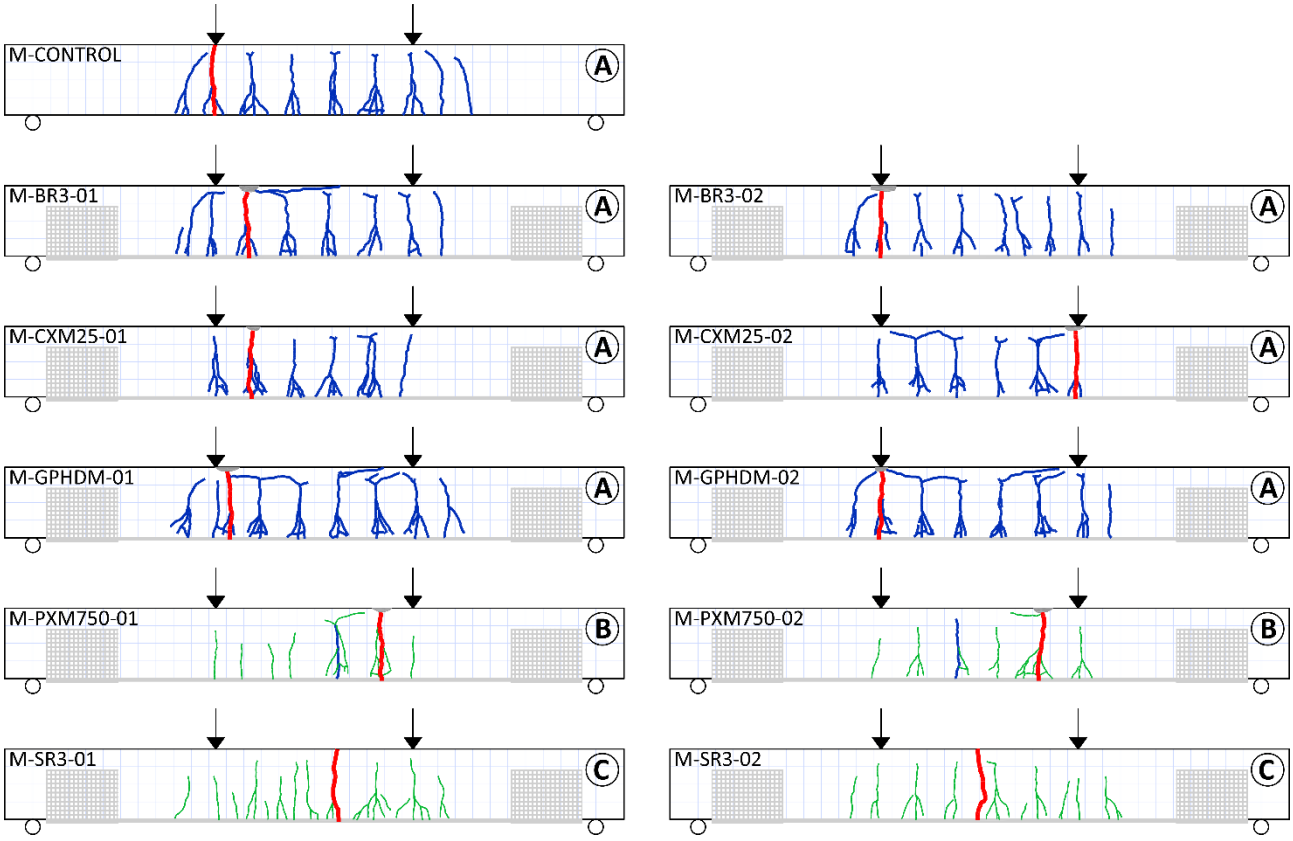

Figure 6. Cracking patterns of tested beams.

Table 5 summarises the results obtained in the experimental campaign. This table contains the cracking pattern, the experimental values of the ultimate flexural moment ($M_{u,exp}$), the yielding flexural moment ($M_{y,exp}$) and the acting flexural moment at the first-crack ($M_{cr,exp}$) developed in the middle-section of the beams, the corresponding increment values of the strengthened beams regarding the control beam ($\Delta M_{u,exp}$, $\Delta M_{y,exp}$, $\Delta M_{cr,exp}$). It is worth mentioning that the self-weight of the beams as well as the weight of the steel distribution beam were took into account to determine the values of the flexural moment results. Regarding the experimental value of the acting flexural moment at first-crack ($M_{cr,exp}$), it was obtained as the value of the flexural moment when the first discontinuity in the moment versus mid-span deflection diagram occurred. Notice that these values were not included in those beams which were cracked previously to be tested. On the other hand, vertical displacement of the middle-section at the ultimate flexural moment (δ_u) and at the yielding flexural moment (δ_y) are also included in Table 5. The last column of the Table 5 corresponds to FRCM strengthening thickness (g).

Table 5. Summary of the experimental results.

Specimen	*Cracking pattern*	$M_{u,exp}$ (kNm)	$M_{y,exp}$ (kNm)	$M_{cr,exp}$ (kNm)	$\Delta M_{u,exp}$ (%)	$\Delta M_{y,exp}$ (%)	$\Delta M_{cr,exp}$ (%)	$\delta_{u,exp}$ (mm)	$\delta_{y,exp}$ (mm)	*g* (mm)
M-CONTROL	A	67.89	48.66	30.02	-	-	-	135.08	10.05	-
M-BR3-01	A	77.72	59.32	43.28	14	22	44	122.99	14.43	8.40
M-BR3-02 (*)	A	72.37	57.92	-	7	19	-	118.56	15.76	6.10
M-CXM25-01 (*)	A	70.28	59.26	-	4	22	-	117.78	16.36	7.50
M-CXM25-02	A	72.96	60.98	33.13	7	25	10	123.10	16.23	6.00
M-GPHDM-01	A	74.55	57.79	46.64	10	19	55	145.63	13.27	6.50
M-GPHDM-02	A	70.16	58.29	41.50	4	19	38	110.72	15.81	9.30
M-PXM750-01	B	64.54	64.24	35.86	-5	32	19	69.74	21.92	9.10
M-PXM750-02 (*)	B	67.98	62.87	-	0	29	-	50.95	18.85	6.90
M-SR3-01	C	80.43	70.56	42.33	18	45	41	46.52	24.58	5.30
M-SR3-02 (*)	C	83.77	68.73	-	23	41	-	46.43	21.07	7.20

(*) Beams flexural-cracked previously to be tested.

Figure 7 shows the experimental curves of the bending moment developed in the middle of the beam (*M*) versus the vertical displacement at the mid-span section (δ) of all specimens for each cracking pattern. The data of the unstrengthened control beam (M-CONTROL) is included in all the cases for comparison purposes.

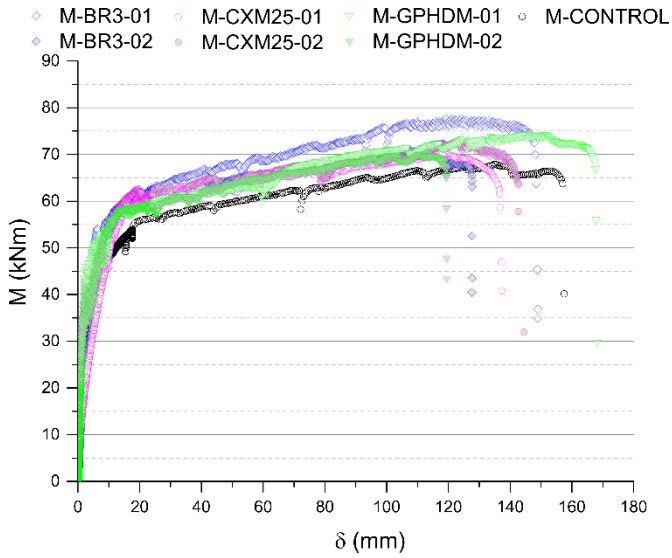

(a)

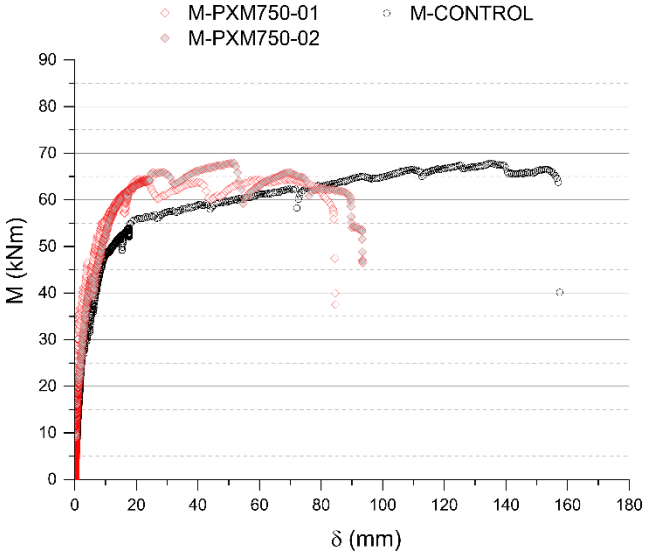

(b)

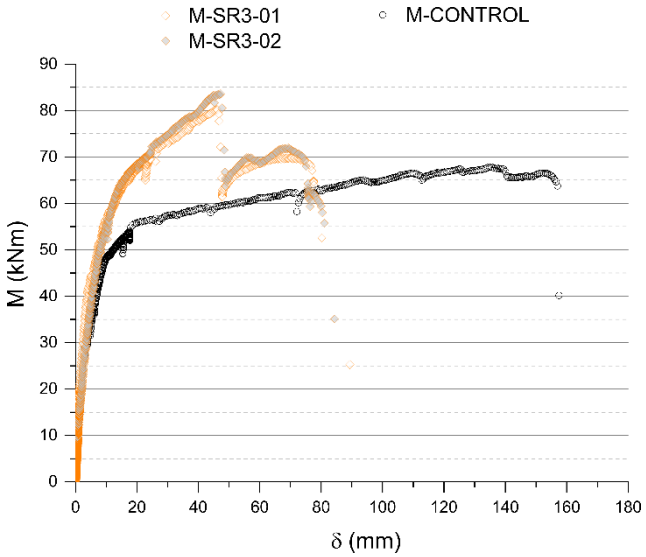

(c)

Figure 7. Bending moment vs. vertical displacement of the mid-span section: (a) cracking pattern A, (b) cracking pattern B and (c) cracking pattern C. The unstrengthened beam is included in all the cases.

According to the values showed in Table 5, the results of the normalized increment of ultimate flexural moment ($\Delta M_{tex,u}$) and the normalized increment of yielding flexural moment ($\Delta M_{tex,y}$) were calculated for each strengthened beam tested. These values are summarized in the third and the fourth column of the Table 6.

Figure 8 shows the ductility (χ) developed by the M-beams during the loading process. Last column of Table 6 includes the reduction of the ductility of the strengthened beams with respect to the control beam ($\Delta\chi$). Additionally, the cracking pattern is also included in Table 6.

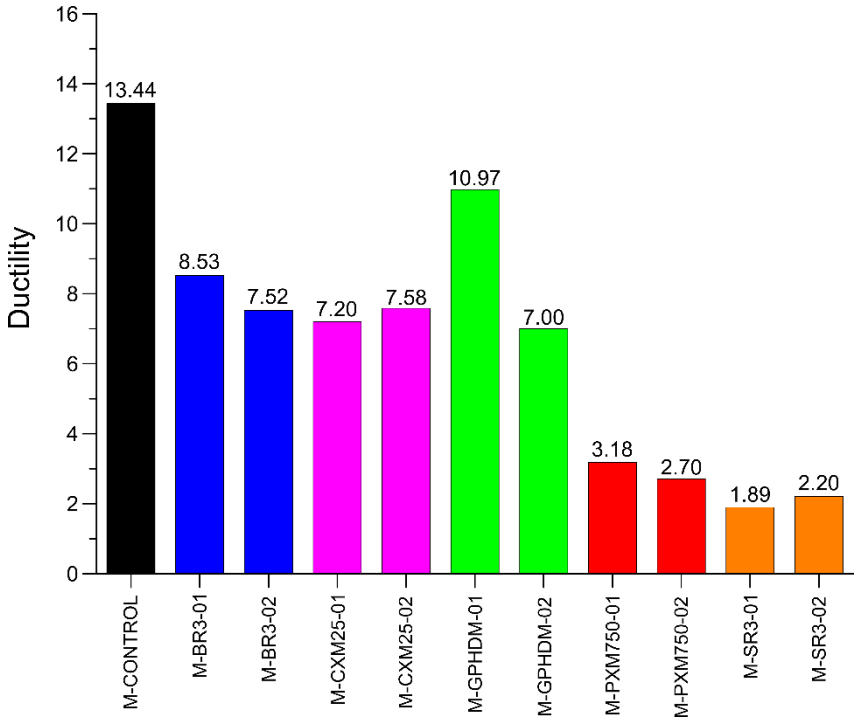

Figure 8. Ductility of the tested M-beams.

Table 6. Normalized increment of ultimate flexural moment, normalized increment of yielding flexural moment and decrement of the ductility.

Specimen	*Cracking pattern*	$\Delta M_{tex,u}$ *(%)*	$\Delta M_{tex,y}$ *(%)*	$\Delta\chi$ *(%)*
M-BR3-01	A	60	65	37
M-BR3-02	A	27	56	44
M-CXM25-01	A	11	47	46
M-CXM25-02	A	22	54	44
M-GPHDM-01	A	61	83	18
M-GPHDM-02	A	21	87	48
M-PXM750-01	B	-	58	76
M-PXM750-02	B	0	53	80
M-SR3-01	C	52	91	86
M-SR3-02	C	66	83	84

Regarding the flexural stiffness analysis, Figure 9 includes the applied-force versus mid-span deflections diagrams of those beams which were not cracked previously to test. Furthermore, the idealized lines which best fit the mechanical behaviour of the specimens are also plotted and the constitutive equation of each line is included.

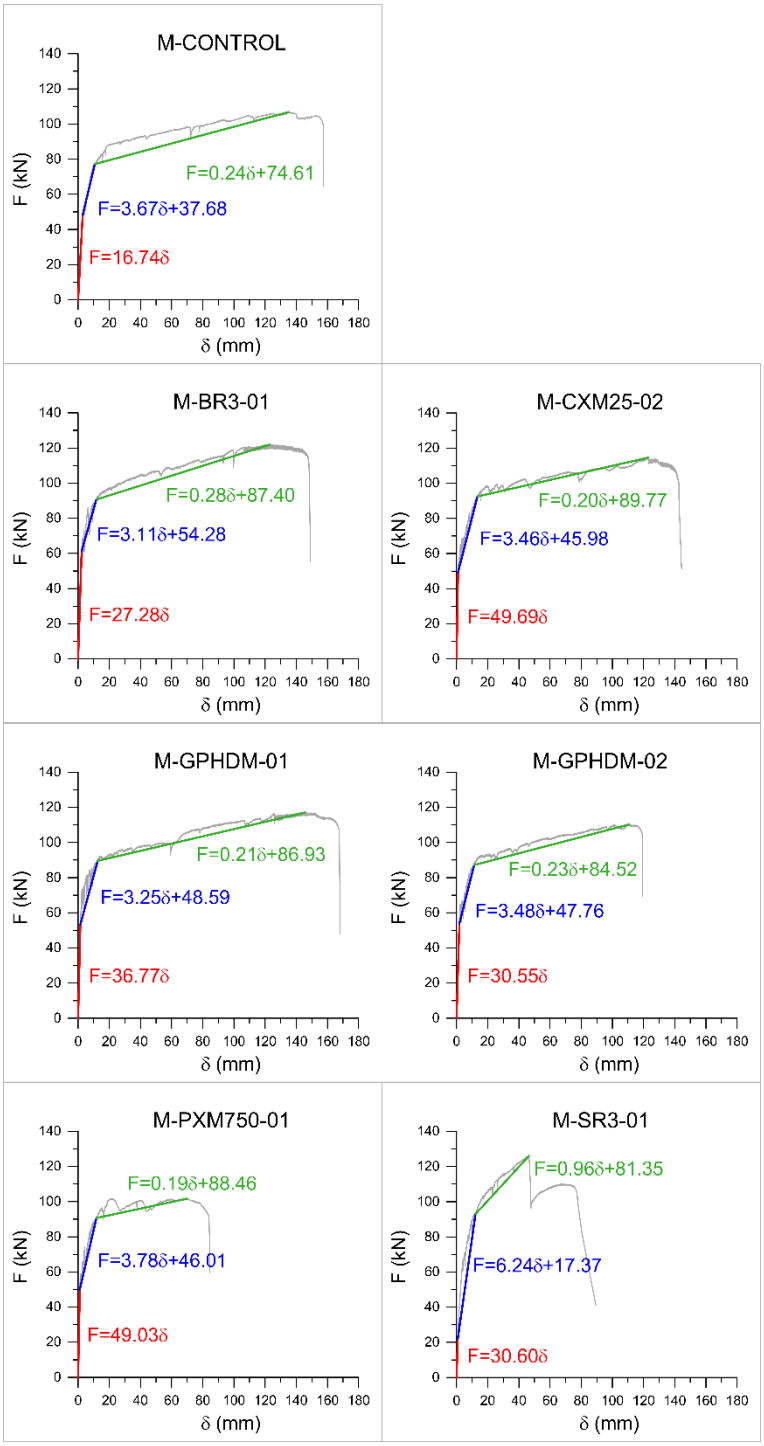

Figure 9. Applied-force versus mid-span deflections of the M-beams which were not cracked previously tot test. Experimental curves and the corresponding idealized behaviour lines.

Table 7 includes the flexural stiffness (*EI*) values of the not pre-cracked M-beams for all the loading stages analysed. For each strengthened beam, this table also contains the increasing or decreasing percentage value of flexural stiffness (*ΔEI*) regarding the unstrengthened specimen.

Table 7. Flexural stiffness of the not pre-cracked M-beams and increasing or decreasing percentage regarding M-CONTROL beam. Values for linear elastic, post-cracked and post-yield stages.

Specimen	*Linear elastic*		*Post-cracked*		*Post-yield*	
	EI (MNm²)	*ΔEI (%)*	*EI (MNm²)*	*ΔEI (%)*	*EI (MNm²)*	*ΔEI (%)*
M-CONTROL	18.70	-	4.10	-	0.27	-
M-BR3-01	30.47	63	3.47	-15	0.31	17
M-CXM25-02	55.50	197	3.86	-6	0.22	-17
M-GPHDM-01	41.07	120	3.63	-11	0.23	-13
M-GPHDM-02	34.12	83	3.89	-5	0.26	-4
M-PXM750-01	54.76	193	4.22	3	0.21	-21
M-SR3-01	34.18	83	6.97	70	1.07	300

As it has been previously mentioned, three different cracking patterns were observed during the tests. Figure 10 shows a zoom of the post-cracked stage in the flexural moment versus mid-span deflection diagrams of the M-beams. On the other hand, in Figure 11 could be observed the strain distribution along the tensile side of the beams for different loads. In this figure is represented one strengthened beam for each cracking pattern developed. Moreover, in all the cases the strain distribution of the unstrengthened specimen is also included. Note that those beams which cracked previously to test are not included in the study of the cracking process.

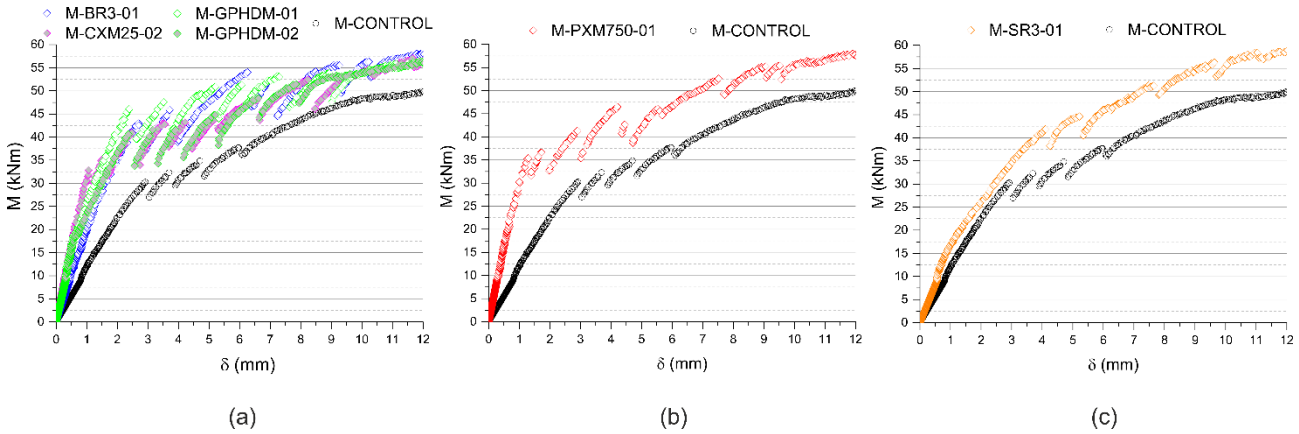

Figure 10. Post-cracked stage of M-beams: (a) cracking pattern A, (b) cracking pattern B and (c) cracking pattern C. The unstrengthened beam is included in all the cases.

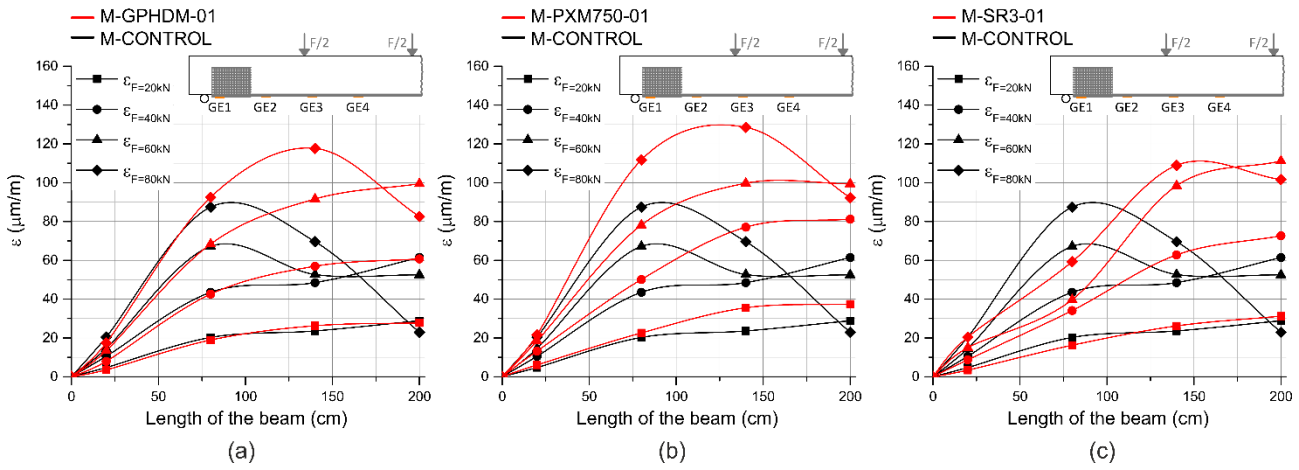

Figure 11. Tensile strains of M-beams: (a) cracking pattern A, (b) cracking pattern B and (c) cracking pattern C. The unstrengthened beam is included in all the cases.

Finally Table 8 shows the experimental values of the acting flexural moment at first-crack ($M_{cr,exp}$) (also included in the fifth column of the Table 5), the theoretical values of the acting flexural moment at first-crack without taking into account the externally bonded reinforcement ($M_{cr,0}$) obtained from evaluating equations Eq. 8 and Eq. 9, and the increasing of the acting flexural moment at first-crack because of FRCM ($\Delta M_{cr,FRCM}$) calculated using equation Eq. 7.

Table 8. Experimental and theoretical acting flexural moment at first-crack, and increasing of the acting flexural moment at first-crack because of FRCM

Specimen	$M_{cr,exp}$ *(kNm)*	$M_{cr,0}$ *(kNm)*	$\Delta M_{cr,FRCM}$ *(kNm)*
M-CONTROL	30.02	29.87	~0.00
M-BR3-01	43.28	37.07	6.21
M-CXM25-02	33.13	29.90	3.23
M-GPHDM-01	46.64	32.30	14.34
M-GPHDM-02	41.50	32.32	9.18
M-PXM750-01	35.86	29.87	5.99
M-SR3-01	42.33	32.27	10.06

5. Comparison and discussion

In general terms, it is important to highlight that exists a relationship between the cracking pattern and type of FRCM applied as a flexural reinforcement (Figure 6 and Table 5). In these terms it is noticeable that the beams strengthened with basalt, carbon and glass grids developed the same cracking pattern than the unstrengthened beam (cracking pattern A). Regarding the M-PXM750 specimens, only two cracks grew during the loading procedure (cracking pattern B). Similarly, beams reinforced with steel meshes had the same cranking process in which just one crack opened (cracking pattern C). This relationship may be caused by two reasons: first, matrices developed scattered levels of adherence with respect to their corresponding textiles at early stages of load, and second, some textiles presented a better performance to distribute stresses during the cracking process than the others.

Following subsections include the discussion about the different analysed variables described in section 3 and the comparison of the mechanical behaviour developed by RC beams flexural strengthened with different types of FRCM.

5.1 Flexural capacity

According to the results showed in Table 5, it can be observed that all the strengthened beams were able to increase the experimental values of the acting flexural moment at first-crack ($M_{cr,exp}$) and the yielding flexural moment ($M_{y,exp}$) with respect to the unstrengthened beam. With regard to the experimental ultimate flexural moment ($M_{u,exp}$), most of the strengthened specimens reached higher values than M-CONTROL. Nevertheless, that was not the case of the beams flexural strengthened with PBO meshes, where the increment of the experimental ultimate flexural moment with respect to the control beam ($\Delta M_{u,exp}$) were non-existent or even negative. This phenomenon was also observed by Ombres [10] and D'Ambrisi and Focacci [24] in their investigations carried out with RC beams flexural strengthened with PXM750 reinforcement system. In spite of being necessaries more specific researches in this way, the ineffectiveness of this type of FRCM to increase the ultimate capacities of the beams may be due to the debonding and the significant slipping of the fibres inside the matrix. This slipping was quantified by D'Ambrisi and Focacci [24] from 1 mm up to 2 mm in the sections where the maximum bending moment were developed.

Analysing Figure 7 could be observed that the specimens with the same cracking pattern developed similar mechanical behaviours. In particular, M-SR3 beams were these ones that reached highest values of ultimate bending moment ($M_{u,exp}$) and yielding bending moment ($M_{y,exp}$) with an average increasing of 21% and 43%, respectively (Figure 7c and Table 5).

As it has been mentioned previously, specimens strengthened with PBO textiles were not able to increase the ultimate capacity of the unstrengthened beam. However, these beams were the ones which developed the second high increase of the linear capacity previous to yield with an average increment with respect to M-CONTROL of 31% (Figure 7b and Table 5).

Observing Figure 7a may be mentioned that all the beams which developed the cracking pattern A had a similar post-yield behaviour between them and also with respect to the control beam. Different types of FRCM provided an increasing of the yielding flexural moment ($\Delta M_{y,exp}$) comprised between 19% and 25% (column 7 of Table 5) and an increasing of the ultimate flexural moment ($\Delta M_{u,exp}$) comprised between 3% and 14% (column 6 of Table 5). These results suggested that these strengthening systems are more reliable in increasing the yielding flexural capacities than the ultimate flexural capacities. Similarly to the case of PBO beams, this phenomenon could be explained because of the slipping of the fibres into the matrix due to the progressive opening of the cracks [24] or the rupture of the fibres of the mesh because of their friction with the mortar during the loading process [25–28].

Regarding the efficiency of the different types of FRCM in enhancing the flexural capacity of the RC beams, comparing the results included in the third and the fourth column of the Table 6, it could be affirmed that the reinforcement that behave more efficient was SR3, developing averages of normalized increments of ultimate flexural moment ($\Delta M_{tex,u}$) and yielding flexural moment ($\Delta M_{tex,y}$) about 59% and 87%, respectively. By contrast, the strengthening which presented the worst results in terms of efficiency were PXM750 and CXM25. FRCM based on basalt textiles and glass textiles showed a significant scattering of the results of the normalized increment of ultimate flexural moment ($\Delta M_{tex,u}$). However, their normalized enhancing capacities regarding the yielding flexural moment were above 50%. It is noteworthy the case of the GPHDM: despite the beams strengthened with this reinforcement developed the lower absolute increment of yielding flexural moment, it showed a level of efficiency similar to SR3 reinforcement.

5.2 Ductility

As is stated in Figure 8, it could be observed that all the strengthened specimens developed lower level of ductility than the control beam. This fact may be explained because the mid-span deflection of strengthened beams when started to yield were generally higher than the unstrengthened one, whereas the mid-span deflection of the control beam at the ultimate flexural moment was higher than the developed by the specimens reinforced with FRCM. This singularity implies that the appliance of the FRCM as a flexural strengthening may bring a reduction of the security level of RC beams because the amount of the allowed deflection between the yielding stage and the ultimate stage is also reduced.

The results included in Figure 8 and fourth column of the Table 6 suggest that exists a relationship between the cracking pattern and the degree of reduction of the ductility. In particular, the beams which developed cracking pattern B (M-PXM750) or cracking pattern C (M-SR3) developed ductility reductions above 76%. By contrast, the ductility decreasing of those beams which developed cracking pattern A were comprised between 18% and 48%.

5.3 Flexural stiffness

Despite the influence of the modulus of the elasticity of the concrete were not took in to account in this analysis, the obtained values are useful to see general behaviour trends of the applied composite reinforcements regarding the flexural stiffness of the whole structure. The changes caused by FRCM in the flexural stiffness of the RC beams were studied in the three stages of the loading process.

According to the results included in Figure 9 and Table 7, the bonded strengthening system provided an increasing of the flexural stiffness, especially in the linear elastic stage. This fact suggests that the different applied types of FRCM were activated at low stages of low and indicates that may not be necessary to prestress the textiles in order to reduce the deflections caused by loads in existing structures. In contrast with this, most of the FRCM were not be able to provide an increasing of the flexural stiffness regarding unstrengthened beam in post-cracked and post-yield stage. This is in accordance with the evidences found in the flexural capacity analysis in which the different FRCM strengthening showed less effective as the applied load increased. However, there is one exception to this trend: in the case of SR3 strengthening, the highest flexural stiffness increment was during the post-yield stage. This behaviour is supported by the fact that steel filaments did not break due to the friction with the mortar during the cracks opening and neither presented large slips.

Comparing the different specimens, only the SR3 type provided to RC beams an increment of flexural stiffness in all the loading stages analysed. Concerning the linear elastic stage, the specimens which developed the highest increase of flexural stiffness were M-CXM25-02 and M-PXM750-01. Specifically, the results obtained by these specimens doubled the flexural stiffness developed by the unstrengthened beam (Table 7). On the other hand, the beam strengthened with basalt textiles was the specimen which obtained the lower value of increment in flexural stiffness.

5.4 Cracking processes

The results obtained in the experimental campaign suggest that FRCM delays the appearance of the first flexural crack. In the graphs included in Figure 10 can be observed that the first discontinuity in the bending moment-deflection diagrams of the strengthened beams appeared at higher values of bending moment than the unstrengthened specimen.

Furthermore, it may also be noticed that there is a certain relationship between the cracking pattern developed by the specimens and the amount of discontinuities presented in the bending moment-deflection diagrams (Figure 10). In this sense, specimens with cracking pattern A (Figure 10a) presented a higher amount of discontinuities than those specimens which developed cracking pattern B (Figure 10b) or cracking pattern C (Figure 10c).

Regarding the behaviour of tensile side of the beams, it could be noticed that measured values of the strains in the cracking area depended on the type of FRCM used, especially at values of applied load above 40 kN (Figure 11). In most of the cases, when this load was overpassed, cracking started particularly in the middle span between loading application sections. Then, the strains of the areas located between two consecutive cracks were reduced because of the opening of these cracks. In particular, it could be observed in Figure 11 that this phenomenon started earlier in control beam than the strengthened ones. Furthermore, the delay of loss of strain due to cracking seems that is more significant in these beams which developed cracking pattern C (Figure 11c) and cracking pattern B (Figure 11b).

Analysing the increment of the acting flexural moment at first-crack because of FRCM ($\Delta M_{cr,FRCM}$) included in Table 8, it could be observed that, in all the cases, FRCM strengthening allowed to increase the value of the flexural moment at the first crack. Considering that the increment of the acting flexural moment at first-crack of the unstrengthened beam was nearly zero, it seems that this method to quantify the starting

of the cracking is reliable. Comparing the different FRCM materials, those which were casted with glass and steel grids presented the better performance on delaying the appearance of the first crack. On the other hand, carbon FRCM was the strengthening system that provide lower levels of increment of the acting flexural moment at first-crack.

6. Conclusions

This work presents an experimental study about the mechanical behaviour of RC beams flexural strengthened with five types of FRCM and subjected to bending tests. In this, flexural capacity and effectiveness of the different strengthening systems are studied. Additionally, the ductility and the flexural stiffness developed by the specimens during the tests are investigated. Finally, a detailed analysis of the cracking processes occurred during the loading stages is also included.

In accordance with the experimental campaign carried out, it is worth to notice that removing the fine grain of the concrete surface and anchoring the FRCM by means of U-jacket FRCM systems arranged at the ends of the external flexural reinforcement perform properly in order to avoid debonding failures between the strengthening and the substrate.

Results suggest that the type of FRCM applied as a flexural strengthening affects the cracking pattern of the tested beams. In this sense, it can be said that steel and PBO-FRCM systems allow the strengthened beams to change the cracking pattern with respect to the control beam. It is important to highlight this phenomenon because the analysis of the different variables shows that there is a relationship between the cracking pattern and the mechanical behaviour of the strengthened specimens.

Analysing the flexural capacity, all FRCM studied materials provide to the RC beams increments of acting flexural moment at the first-crack and yielding flexural moment with respect to unstrengthened beam, with an average increasing about 35% and 27%, respectively. However, this was not the case regarding ultimate flexural moment, where specimens strengthened with PBO-FRCM did not reach the ultimate bending capacity developed by the control beam. These results lead to the conclusion that the ultimate flexural capacity of FRCM strengthened beams is highly affected by the bonding capacity between meshes and matrices.

According to the obtained results, FRCM materials applied as flexural strengthening reduce the ductility of the reinforced concrete beams, being this phenomenon more pronounced in those specimens which developed cracking patterns with less opening of the cracks. This could lead a loss of the security level of the strengthened structures and should be taken into account in the design of this type of strengthening solutions.

The study of the flexural stiffness shows that FRCM increases the rigidity of the beams, especially in the linear elastic stage where an average increasing of 135% with respect to unstrengthened beam was obtained. Thus, it could be affirmed that FRCM applied as a flexural strengthening could reduce the deflections during initial stages of loading.

Finally, all of the evidences showed above suggest that applying FRCM as a flexural strengthening could delay the appearance of the first crack and reduce the cracking of RC concrete beams subjected to an increasing loading process, especially in the cases where glass or steel grids are used.

In reference to the comparison among the different strengthening materials, it can be said that steel composite was the FRCM that performed best in terms of increasing the flexural capacity. Furthermore, it was the only strengthening which offered an increasing of the flexural stiffness during all the stages of

loading. Despite of this, beams externally reinforced with SR3 were those ones which developed highest decreasing of ductility. Although specimens strengthened with PBO meshes performed second best results on improving the yielding flexural capacity of the beams, they were not able to enhance the ultimate flexural moment. It suggests that this FRCM suffers of a lack of adherence between the grid and the matrix. Analysing BR3 and CXM25, both basalt and carbon based materials offered similar behaviours in terms of increasing the flexural capacity and reducing the ductility. However, it should be noted that C-FRCM was the best strengthening on enhancing the flexural stiffness during the linear elastic stage of loading. Finally, despite GPHDM composites provided strengthened beams the lower enhancing of yielding flexural moment, the effectiveness of this FRCM was similar to SR3 strengthening. Moreover, M-GPHDM beams were the specimens that showed more efficiency on delaying the appearance of the first crack, achieving an average increasing of the acting flexural moment at first-crack because of FRCM over 11%.

References

[1] L. Garmendia, J.T. San-José, D. García, P. Larrinaga, Rehabilitation of masonry arches with compatible advanced composite material, Construction and Building Materials. 25 (2011) 4374–4385.

[2] E. Bernat, L. Gil, P. Roca, C. Escrig, Experimental and analytical study of TRM strengthened brickwork walls under eccentric compressive loading, Construction and Building Materials. 44 (2013) 35–47.

[3] T.C. Triantafillou, C.G. Papanicolaou, Shear strengthening of reinforced concrete members with textile reinforced mortar (TRM) jackets, Materials and Structures. 39 (2006) 93–103.

[4] C. Escrig, L. Gil, E. Bernat-Maso, F. Puigvert, Experimental and analytical study of reinforced concrete beams shear strengthened with different types of textile-reinforced mortar, Construction and Building Materials. 83 (2015) 248–260.

[5] T.C. Triantafillou, C.G. Papanicolaou, Textile reinforced mortars (TRM) versus fibre reinforced polymers (FRP) as strengthening materials of concrete structures, in: Proceedings of the 7th ACI International Symposium on Fibre-Reinforced (FRP) Polymer Reinforcement for Concrete Structures, 2005: pp. 99–118.

[6] S. Kurtz, P. Balaguru, Comparison of inorganic and organic matrices for strengthening of RC beams with carbon sheets, Journal of Structural Engineering. (2001) 35–42.

[7] H. Toutanji, Y. Deng, Comparison between organic and inorganic matrices for RC beams strengthened with carbon fiber sheets, Journal of Composites for Construction. 11 (2007) 507–513.

[8] A. Si Larbi, R. Contamine, P. Hamelin, TRC and hybrid solutions for repairing and/or strengthening reinforced concrete beams, Engineering Structures. 45 (2012) 12–207–534.

[9] A. Brückner, R. Ortlepp, M. Curbach, Textile reinforced concrete for strengthening in bending and shear, Materials and Structures. 39 (2006) 741–748.

[10] L. Ombres, Flexural analysis of reinforced concrete beams strengthened with a cement based high strength composite material, Composite Structures. 94 (2011) 143–155.

[11] S. Babaeidarabad, G. Loreto, A. Nanni, Flexural strengthening of RC beams with an externally bonded fabric-reinforced cementitious matrix, Journal of Composites for Construction. 18 (2014) 1–12.

[12] A. D'Ambrisi, F. Focacci, Flexural strengthening of RC beams with cement-based composites, Journal of Composites for Construction. 15 (2011) 707–720.

[13] U. Ebead, K.C. Shrestha, M.S. Afzal, A.E. Refai, A. Nanni, Effectiveness of Fabric-Reinforced Cementitious Matrix in Strengthening Reinforced Concrete Beams, Journal of Composites for Construction. 04016084 (2016) 1–14.

[14] H.M. Elsanadedy, T.H. Almusallam, S.H. Alsayed, Y.A. Al-Salloum, Flexural strengthening of RC beams using textile reinforced mortar – Experimental and numerical study, Composite Structures. 97 (2013) 40–55.

[15] P. Larrinaga, J.T. San-José, D. García, L. Garmendia, J. Díez, Experimental study of the flexural behaviour of low performance RC beams strengthened with textile reinforced mortar, in: International Rilem Conference on Material Science and 64th RILEM Annual Week in Aachen - MATSCI 1. 75, 2010: pp. 235–244.

[16] L. Gil, C. Escrig, E. Bernat, Bending performance of concrete beams strengthened with textile reinforced mortar TRM, Key Engineering Materials. 601 (2014) 203–206.

[17] Comité Européen de Normalisation, EN 12390-1. Testing hardened concrete - Part 1: Shape, dimensions and other requirements for specimens and moulds, (2012).

[18] Comité Européen de Normalisation, EN 12390-3. Testing hardened concrete - Part 3: Compressive strength of test specimens, (2009).

[19] Comité Européen de Normalisation, EN ISO 15630-1. Steel for the reinforcement and prestressing of concrete. Test methods - Part 1: Reinforcing bars, wire rod and wire, (2010).

[20] Comité Européen de Normalisation, EN 1015-11. Methods of test for mortar for masonry - Part 11: Determination of flexural and compressive strength of hardened mortar, (1999).

[21] E. Bernat, Analysis of unreinforced and TRM-strengthened brickwork walls with eccentric axial load applied, Phd Thesis. Department of Strength of Materials and Engineering Structures. Universitat Politècnica de Catalunya, BarcelonaTECH, 2013.

[22] A. Brückner, R. Ortlepp, M. Curbach, Textile reinforced concrete for strengthening in bending and shear, Materials and Structures. 39 (2006) 741–748.

[23] Comisión Permanente del Hormigón, EHE-08-Instrucción para el proyecto y ejecución de obras de hormigón en masa y armado, (2008).

[24] A. D'Ambrisi, L. Feo, F. Focacci, Experimental analysis on bond between PBO-FRCM strengthening materials and concrete, Composites Part B: Engineering. 44 (2013) 524–532.

[25] A. Badanoiu, J. Holmgren, Cementitious composites reinforced with continuous carbon fibres for strengthening of concrete structures, Cement and Concrete Composites. 25 (2003) 387–394.

[26] B. Banholzer, T. Brockmann, W. Brameshuber, Material and bonding characteristics for dimensioning and modelling of textile reinforced concrete (TRC) elements, Materials and Structures. 39 (2006) 749–763.

[27] U. Häußler-Combe, J. Hartig, Bond and failure mechanisms of textile reinforced concrete (TRC) under uniaxial tensile loading, Cement and Concrete Composites. 29 (2007) 279–289.

[28] B. Zastrau, I. Lepenies, M. Richter, On the Multi Scale Modeling of Textile Reinforced Concrete Micro scale Meso scale Macro scale, Technische Mechanik. (2008) 53–63.

List of tables

List of figures